ACS APPLIED MATERIALS & INTERFACES

Forum Article

www.acsami.org

Poly(*N*-isopropylacrylamide)-Based Mixed Brushes: A Computer Simulation Study

Fabien Léonforte* and Marcus Müller*

Institut für Theoretische Physik, Georg-August-Universität, Friedrich-Hund-Platz 1, 37077 Göttingen, Germany

ABSTRACT: Temperature-sensitive poly(*N*-isopropylacrylamide) (PNIPAM) polymer brushes of fixed molecular weight and grafting density are modeled in the framework of a coarse-grained model with soft, nonbonded interactions and an implicit solvent. This model has been developed to address experimentally relevant, large invariant degrees of polymerization, and nonbonded interactions are expressed via a third-order (virial) expansion of the equation of state. The choice of interaction parameters is intended to mimic the swelling behavior of PNIPAM in water as the temperature increases toward the lower critical solution temperature (T^{LCST}). Results of molecular dynamics simulations for one component brushes are compared to experimental data. Mixed brushes incorporating small and large amounts of grafted poly(ethylene glycol) polymers are then considered. The effects of mixing polymer components on the response of the mixed brushes to temperature changes are monitored, and the results are compared to experimental data. In the end, two design principles for biomolecule triggering using temperature-sensitive mixed polymer brushes with functional and switchable end-groups are proposed and studied. This work is in favor of establishing qualitative rules for the design, optimization, and comprehension of binary polymer brushes for bioengineering purposes.

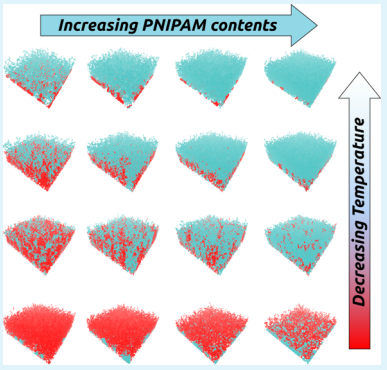

KEYWORDS: *molecular dynamics simulations, DPD thermostat, implicit solvent, thermo-responsive polymers, functional end-groups, biomolecules*

1. INTRODUCTION

End-grafted water-soluble poly(*N*-isopropylacrylamide) (PNIPAM) polymer brushes are promising for the fabrication of responsive surfaces due to their reduced swelling above a lower critical solution temperature (T^{LCST}) estimated to be ∼305.15 K (32 °C).[1−3] Below the T^{LCST}, the polymer chains are swollen with water, whereas above it, dehydration effects drive the polymer components to form more compact structures that depend on the grafted density of the brush.[4] On the basis of this phase transition, grafted PNIPAM brush surfaces display increased hydrophobicity[5] and reduced layer thickness[6] above the T^{LCST}. Several aspects of the polymers can alter the thermal response of the brush. For example, the molecular weight impacts the initial swollen state of the brush (less swelling at higher molecular weights); furthermore, an increase in the temperature range of switching is observed when the grafting density is decreased.[7]

Interest in PNIPAM thermoresponsive polymers has arisen because the T^{LCST} is close to the physiological temperature of humans. Therefore, modifications of the bulk substrate with polymers such as PNIPAM are extremely important for emerging medical and biological technologies. For instance, PNIPAM has been successfully utilized to control protein adsorption as well as cell attachments.[8−12] Additionally, PNIPAM-modified substrates (multicomponent polymer brushes) enable the harvesting of confluent cell sheets as well as the release of said cell sheets through simple control of the environmental temperature.

For this purpose, good protein resistance for polymer brushes can be achieved by mixing PNIPAM with water-soluble poly(ethylene glycol) (PEO) polymers. This strategy was previously proposed for microgel particles in which PEO was employed as a cross-linker of linear PNIPAM.[13,14] PEO polymers are water-soluble, biocompatible, nontoxic, and nonimmunogenic; they can be used as grafted chains, and their role in the controlled release of macromolecular objects can be crucial.[15] Because of their large excluded volume, PEO components in brushes exhibit a repulsive osmotic interaction when penetrated by proteins or cells, and they have been shown to provide a steric repelling barrier against protein adsorption.[16] Furthermore, because of their high hydration rate, PEO polymers can boost drug release when they are mixed with some other species.[15] Therefore, understanding the behavior of mixed PNIPAM:PEO polymer brushes is prerequisite for using such systems in on-demand drug delivery applications.

It was recently shown that PEO polymers demonstrate complex intricate behaviors when mixed with other water-soluble polymers. Indeed, like PNIPAM, PEO also forms hydrogen bonds with water that could interfere with interactions of PNIPAM with itself and with water.[17] In particular, it has been

Special Issue: Forum on Polymeric Nanostructures: Recent Advances toward Applications

Received: November 3, 2014
Accepted: January 21, 2015
Published: January 29, 2015

DOI: 10.1021/am5076309
ACS Appl. Mater. Interfaces 2015, 7, 12450−12462

shown that hydrophobically driven adsorption of proteins can be avoided by the creation of a protective hydration shell that is due to specific PEO−water hydrogen bonding.[14,18,19] Furthermore, in recent works by Seeber et al.,[17] intriguing behaviors have been observed. It was shown that PNIPAM:PEO mixed brushes swell less when the species are mixed, that both species seem to interact at all temperatures (though less at $T < T^{LCST}$), and that even a small amount of PEO in a PNIPAM brush can have a strong effect on the ability of PNIPAM to exhibit a thermal response. In the latter study, protein adsorption was quasi-suppressed even at $T > T^{LCST}$ due to the creation of hydrophilic surfaces by PEO components that extend outward from the brush and sustain solubility by reducing the collapse of the PNIPAM component. Here, we will conceptually address these issues as a function of graft density in which PNIPAM and PEO become increasingly mixed.

The challenge in modeling stimuli-responsive polymeric systems is in trying to account for the subtle interplay between their chemo- and physicomechanical properties and to capture the involved collective mechanisms without the loss of relevant details and within an accessible computational time and length scale. The choice of the simulation model used to describe the stimuli-responsive polymer and its interaction with the solvent is therefore crucial. In the framework of standard particle-based simulations, one method is to develop a coarse-graining procedure that decimates irrelevant degrees of freedom of the polymer[20−22] and accounts for the solvent either implicitly (e.g., by tuning the interaction range of the pair potential)[23,24] or by including it explicitly,[25,26] which is probably more realistic but slows the computational efficiency and limits the size of the systems.

Another way to access experimentally large and invariant degrees of polymerization, accounting for realistic fluctuations, is to make use of coarse-grained polymers with soft, nonbonded interactions.[27,28] Within the framework of molecular dynamics (MD) simulations with a dissipative-particle-dynamics (DPD) thermostat, this approach allows us to efficiently equilibrate the morphology at a relatively low computational cost when used in conjunction with a sequential and adaptive cooling procedure and a computationally efficient calculation of the interactions.[29] In contrast to the standard coarse-graining approach in which the solvent is implicitly included through a tunable interaction range in the force field,[24] the aqueous solvent in our model is implicitly expressed through coefficients appearing in a third-order virial expansion of the equation of state (EOS) for the nonbonded interactions.[27,28] Therefore, our model accounts for the molecular characteristics on a coarse-grained level and uses a top-down representation of the interaction of the polymers with their environment via an EOS with experimentally realistic molecular weights.

This paper is organized as follows. In section 2, we provide details of the simulation techniques and describe the coarse-graining procedure. Brushes composed of pure PNIPAM at various molecular weights and grafting densities are studied in section 3. Biocompatible mixes of PNIPAM:PEO brushes are investigated in section 4.1, in which we provide a detailed analysis of the combined effects of grafting densities and the compositional ratio of both species upon temperature-induced swelling of the brush. To make this study viable for experimental purposes, we also provide additional results concerning the effect of polydispersity. In section 4.2, we analyze two experimentally accessible strategies for the development of temperature-sensitive PNIPAM-based mixed brushes for biomolecule triggering or potential drug release. This paper then closes with a brief summary.

2. MODEL AND METHODOLOGY

We employ a coarse-grained model with soft interactions for n Gaussian polymer chains of type A (PNIPAM) and B (PEO). The mixed brushes are composed of $n = \sum_{\alpha=A,B} n_\alpha$ chains, where the molecular contour of a polymer chain contains N_α effective interaction centers (segments). We define the fraction of α polymers in the mixed brush as $f_\alpha = n_\alpha/n$ and the ratio of the size of α species chains to the reference chain length $\bar{N}$ used in the model as $\phi_\alpha = N_\alpha/\bar{N}$. The polymer chains are irreversibly grafted at random positions onto a hard, impenetrable wall located at $r_\perp = 0$.

The explicit degrees of freedom of the solvent are integrated using an equation of state (EOS) formalism.[27,28,30] In this formalism, the effective nonbonded interactions between the polymer segments take the form

$$\frac{\mathcal{H}'_{nb}[\{\mathbf{r}_i(s)\}]}{k_B T} = \int_V \frac{d\mathbf{r}}{R_{ee}^3}\left(\sum_{\alpha,\beta=A,B} \frac{v_{\alpha\beta}}{2}\hat{\rho}_\alpha(\mathbf{r}|\{\mathbf{r}_i(s)\})\hat{\rho}_\beta(\mathbf{r}|\{\mathbf{r}_i(s)\}) + \sum_{\alpha,\beta,\gamma=A,B} \frac{w_{\alpha\beta\gamma}}{3}\hat{\rho}_\alpha(\mathbf{r}|\{\mathbf{r}_i(s)\})\hat{\rho}_\beta(\mathbf{r}|\{\mathbf{r}_i(s)\})\hat{\rho}_\gamma(\mathbf{r}|\{\mathbf{r}_i(s)\})\right) \quad (1)$$

where we define the configuration $\{\mathbf{r}_i(s)\}$ by a set of indexes i and s that run over all of the polymer chains (independent of the polymer species) and all segments of the polymer, respectively. $\hat{\rho}_\alpha(\mathbf{r}|\{\mathbf{r}_i(s)\})$ denotes the dimensionless local density of species α = A, B in volume R_{ee}^3 (which depends explicitly on the particle coordinates), where R_{ee} represents the end-to-end distance of a reference chain with $\bar{N}$ segments. The dimensionless local densities are defined by

$$\hat{\rho}_\alpha(\mathbf{r}|\{\mathbf{r}_i(s)\}) = \frac{R_{ee}^3}{\bar{N}} \sum_{i=1}^{n} \sum_{s=1}^{N_i} \delta[\mathbf{r} - \mathbf{r}_i(s)]\Theta_\alpha(i, s) \quad (2)$$

where $\Theta_\alpha(i,s) = 1$ if the sth segment on the ith polymer chain belongs to species α and 0 otherwise. To regularize the Dirac function in eqs 1 and 2, a weighted-density approximation is used, which leads to a coarse-grained density

$$\tilde{\rho}_{m\alpha}(\mathbf{r}|\{\mathbf{r}_i(s)\}) = \frac{R_{ee}^3}{\bar{N}} \sum_{i=1}^{n} \sum_{s=1}^{N_i} w_m(|\mathbf{r} - \mathbf{r}_i(s)|)\Theta_\alpha(i, s) \quad (3)$$

with weighted functions $w_2(\mathbf{r})$ and $w_3(\mathbf{r})$ defined for the second- and third-order virial contributions in eq 1, respectively, and taking the form

$$w_m(\mathbf{r}) = \frac{15}{2\pi a_m^3}\left(1 - \frac{|\mathbf{r}|}{a_m}\right)^2 \quad (4)$$

for $r \le a_m$ and 0 otherwise. The DPD-like weighting functions defined in eq 4 only differ in their spatial range, and we chose $a_2 = 0.9a_3 \equiv b^{CG}$, where the choice of the Kuhn length b^{CG} for the reference chain will be discussed in section 2.1. The a_m choice is motivated by avoiding liquidlike packing effects of the coarse-grained segments[31,32] that represent multiple atoms along the polymer backbone. Finally, the nonbonded interactions for the free-energy functional (eq 1) in the final form of a coarse-grained multibody DPD model (M-DPD)[31,33−35] Hamiltonian can be rewritten as

$$\frac{\mathcal{H}_{nb}[\{\mathbf{r}_i(s)\}]}{k_B T} = \int_V \frac{d\mathbf{r}}{R_{ee}^3} \sum_{\alpha=A,B,...} \hat{\rho}_\alpha(\mathbf{r}|\{\mathbf{r}_i(s)\}) \left[\sum_{\beta=A,B} \frac{v_{\alpha\beta}}{2}\tilde{\rho}_{2\beta}(\mathbf{r}|\{\mathbf{r}_i(s)\}) + \sum_{\beta,\gamma=A,B} \frac{w_{\alpha\beta\gamma}}{3}\tilde{\rho}_{3\beta}(\mathbf{r}|\{\mathbf{r}_i(s)\})\tilde{\rho}_{3\gamma}(\mathbf{r}|\{\mathbf{r}_i(s)\})\right] \quad (5)$$

DOI: 10.1021/am5076309
ACS Appl. Mater. Interfaces 2015, 7, 12450−12462

In the simulations, the connectivity along the molecular backbone is modeled by a discretized Edwards Hamiltonian for the Gaussian conformations $\{\mathbf{r}_i(s)\}$

$$\frac{\mathcal{H}_b[\{\mathbf{r}_i(s)\}]}{k_BT} = -\sum_{i=1}^{n}\sum_{s=1}^{N-1} 6\ln\left(1 - \left[\frac{\mathbf{r}_i(s) - \mathbf{r}_i(s-1)}{2b^{CG}}\right]^2\right) \quad (6)$$

The bonded interaction between consecutive interaction centers along a chain molecule has a finite extensibility of $b_{max} = 2b^{CG}$ and mean-squared bond length of $(12/17)(b^{CG})^2$. In the absence of nonbonded interactions or geometric constraints, the conformations follow Gaussian statistics characterized by the squared end-to-end distance $R_{eo}^2 = (12/17)R_{ee}^2$. The simulation cell has a lateral extension $L_\parallel = 16R_{ee}$, and periodic boundary conditions are used in the lateral x and y directions. The brush grafting density is defined as $\sigma = n/L_\parallel^2$, which can also be expressed in the dimensional form $\sigma R_{ee}^2 = n/(L_\parallel/R_{ee})^2$. The height of the simulation cell $L_\perp$ is much larger than the height of the brush.

In molecular dynamics (MD) simulations, the classical equations of motion are integrated via the velocity−Verlet algorithm with a time step of $\Delta t = 5 \times 10^{-3}\tau$. The mass of a single bead is set to $m \equiv 1$, and via combination of the units of length and energy (k_BT), the unit of time is $\tau \equiv ((b^{CG})^2/k_BT)^{1/2}$, which can thus be mapped to an experimental time scale. The temperature (T) is kept constant at $k_BT = 1$ using a dissipative particle dynamics (DPD) thermostat,[36,37] which accounts for hydrodynamic interactions due to the local conservation of momentum. The thermostat adds to the total conservative force calculated from eqs 5 and 6, a dissipative force ($\mathbf{F}_i^D$) and a random force ($\mathbf{F}_i^R$) on each monomer i. Both forces are applied in a pairwise manner such that the sum of the thermostating forces acting on a particle pair vanishes. With Γ as the friction constant, the dissipative force is given by

$$\mathbf{F}_i^D = -\Gamma \sum_{j\neq i} \omega^D(r_{ij})(\hat{\mathbf{r}}_{ij}\mathbf{v}_{ij})\hat{\mathbf{r}}_{ij} \quad (7)$$

where $\hat{\mathbf{r}}_{ij} = (\mathbf{r}_i - \mathbf{r}_j)/r_{ij}$ and $\mathbf{v}_{ij} = \mathbf{v}_i - \mathbf{v}_j$. The weighting function is $\omega^D(r_{ij}) = (2\pi(b^{CG})^3/15)w_2(r_{ij})$ (cf. eq 4). The random force is given by

$$\mathbf{F}_i^R = \xi \sum_{j\neq i} \omega^R(r_{ij})\theta_{ij}\hat{\mathbf{r}}_{ij} \quad (8)$$

where θ_{ij} is a random variable with zero mean, unit variance, second moment $\langle\theta_{ij}(t)\theta_{kl}(t')\rangle = (\delta_{ij}\delta_{jl} + \delta_{il}\delta_{jk})\delta(t-t')$ and $\theta_{ij} = \theta_{ji}$. The weight function $\omega^R(r_{ij})$ satisfies the fluctuation−dissipation theorem $[\omega^R]^2 = \omega^D$. Friction Γ and noise strength ξ define the temperature by $\xi^2 = 2k_BT\Gamma$. We chose $\Gamma = 0.5\tau^{-1}$ in all of our simulations. Depending on the grafting density, runs over a period of 350−1000τ are sufficient to achieve the final equilibrated state.

2.1. Coarse-Graining Representation of Polymer Species. To relate the coarse-graining model to a specific polymer molecular, one must account for the conformational differences between the PNIPAM and PEO compounds. To this end, a detailed procedure was followed and is described in ref 30. We first required that the molecular model preserve both the molecular volume (ν_α) and the average, squared end-to-end distance of each species in the coil ($R_{eo}^2(\alpha)$). The molecular volume is related to the experimental monomer number density $\rho_{0(\alpha)}^{exp}$ in the pure phase of the experimental system and the number of repeat units $N_\alpha^{exp} \equiv M_{w(\alpha)}/\mathcal{M}_{w(\alpha)}$, which is the ratio of the molecular weight of the polymer to the molecular mass of the chemical repeat units of the polymer species. Thus, $\nu_\alpha = N_\alpha^{exp}/\rho_{0(\alpha)}^{exp}$. The stoichiometry can be accounted for through the weight fraction ϕ_α such that $\phi_B = 1 - \phi_A$, which, in conjunction with the molecular weight $M_{w(\alpha)}$, allows us to estimate and map the model to the experimental number of molecules per unit volume $n_\alpha/V = (\phi_\alpha/M_{w(\alpha)})[\nu_A\phi_A/M_{w(A)} + \nu_B\phi_B/M_{w(B)}]^{-1}$. Here, we model the polymers as Gaussian chains of statistical segment lengths $b_A^{exp} = 0.38$ nm for PNIPAM and $b_B^{exp} = 0.29$ nm for PEO, whereas the densities of each species in the pure phase are $\rho_{0(A)}^{exp} = 0.95$ g/cm^3 and $\rho_{0(B)}^{exp} = 1.15$ g/cm^3, respectively. Furthermore, the chemical repeat unit masses are $\mathcal{M}_{w(A)} = 113.16$ g/mol for PNIPAM and $\mathcal{M}_{w(B)} = 44.0532$ g/mol for PEO.

The coarse-graining (CG) procedure consists of discretization of the polymer chains by a factor n_{CG}, which aims to map n_{CG} repeated units to one interaction center. Here, PNIPAM polymers represent the reference chains, and discretization leads to rescaling of the statistical segment length $(b_A^{CG})^2 = R_{eo}^2(A)/N_A^{exp}/n_{CG}$, which also defines the reference Kuhn length $b^{CG} \equiv b_A^{CG}$. Hence, species B are also discretized such that $N_B^{CG} = R_{eo}^2(B)/(b_A^{CG})^2$, and the coarse-grained segmental densities for each species are rescaled by the ratio $(b_\alpha^{exp}/b_A^{CG})^2$.

2.2. Implicit Solvent Interaction. The solvent-mediated self-interaction coefficient $\nu_{\alpha\alpha}$ is related to the Flory−Huggins parameters of each species with solvent S via the relation $\chi_{\alpha S}(T) = (1 - (\nu_\alpha^2/\nu_S)\nu_{\alpha\alpha}(T))/2$, which consequently requires the determination of the coefficients $\nu_{\alpha\alpha}$ and $w_{\alpha\alpha\alpha}$ from the characteristic thermodynamic properties of each species. If these coefficients are known for each species, the interspecies compatibility is obtained through the mixing rule[38,39] $\chi_{BA}(T) = (\nu_{ref}/k_BT)(\delta_B(T) - \delta_A(T))^2$, where the segment reference volume ν_{ref} is approximated by $\nu_{ref} \approx (\nu_B\nu_A)^{1/2}$ and δ_B and δ_A are the Hildebrandt solubility parameters.

It follows that the second-order interaction coefficients can be expressed as $\nu_{BA}(T) = [\chi_{BA}(T)(\nu_A\nu_B)^{1/2} + \nu_{AS}(T)\nu_A^2/2 + \nu_{BS}(T)\nu_B^2/2](\nu_A\nu_B)^{-1}$, and the remaining mixed third-order coefficients via mixing of the self-interaction quantities $w_{BBA}(T) = [w_{AAA}(T)w_{BBB}^2(T)]^{1/3}$ and $w_{AAB}(T) = [w_{BBB}(T)w_{AAA}^2(T)]^{1/3}$. For the determination of $w_{\alpha\alpha\alpha}$, we make use of the mean-field EOS for the pure species as

$$\frac{pR_{eo}^3}{k_BT} = \frac{\hat{\rho}_{0(\alpha)}}{\phi_\alpha} + \frac{\nu_{\alpha\alpha}}{2}\hat{\rho}_{0(\alpha)}^2 + \frac{2w_{\alpha\alpha\alpha}}{3}\hat{\rho}_{0(\alpha)}^3 \quad (9)$$

where the dimensionless local density $\hat{\rho}$, which also appears in eq 2, here represents the species density in the pure phase; therefore, it is written as $\hat{\rho}_{0(\alpha)}$. In our solvent-free model, vapor corresponds to the solvent, and we require it to be equal to the coexistence density $\hat{\rho}_{coex(\alpha)}$ at which point the polymeric liquid coexists with its vapor under the assumption that, due to the very low density of the vapor, the pressure at coexistence is approximately null. For our model, this is equivalent to requiring that the polymer phase separate into a dense, polymer-rich phase under poor solvent conditions. Under this assumption, one obtains the relation $\hat{\rho}_{coex(\alpha)} \approx -3\nu_{\alpha\alpha}/4w_{\alpha\alpha\alpha}$. By introducing dimensionless inverse compressibility $\kappa\bar{N} \equiv R_{eo}^3/(\kappa_T\hat{\rho}_{coex(\alpha)}k_BT) = \nu_{\alpha\alpha}\hat{\rho}_{coex(\alpha)} + 2w_{\alpha\alpha\alpha}(\hat{\rho}_{coex(\alpha)})^2$ with $\kappa_T = -(1/V)(\partial V/\partial P)_T$, we arrive at the relations

$$\nu_{\alpha\alpha} = -2\frac{\kappa\bar{N} + 3}{\hat{\rho}_{coex(\alpha)}} \text{ and } w_{\alpha\alpha\alpha} = 3\frac{\kappa\bar{N} + 2}{2\hat{\rho}_{coex(\alpha)}^2} \quad (10)$$

Thus, the third-order self-interaction coefficients for the CG procedure can be obtained by eliminating the inverse compressibility $\kappa\bar{N}$ in eq 10.

3. PNIPAM-BASED HOMOPOLYMER BRUSH

As discussed in section 2.2, the solvent-mediated interaction coefficients encode the knowledge of the thermodynamic properties of the polymer species. In the case of PNIPAM, we aim to reproduce its qualitative thermal response in an aqueous environment. For this purpose, we used the empirical approach developed in ref 40. The model accounts for temperature-dependent alteration of hydrogen bonding of the amide groups of the polymer through the knowledge of an effective Flory−Huggins interaction parameter[41,42] $\chi_{eff}(\Phi,T)$ at a given monomer volume fraction (Φ).

For grafted polymers, the resulting model exhibits a collapse of chains (poor solvent conditions) at $T \geq 303.65$ K, exhibits vertical phase separation in the range $T^{LCST} \leq T \leq 303.65$ K, exhibits good solvent conditions for the brush down to 299.51 K, and exhibits vertical phase separation below the latter temperature only at high grafting densities. On the basis of compiled experimental observations, this model aims to reproduce the thermal response of PNIPAM in the range of 283−343 K and allows us to explicitly obtain expressions for the temperature dependence of the second- and third-order coefficients[43,44] given

DOI: 10.1021/am5076309
ACS Appl. Mater. Interfaces 2015, 7, 12450−12462

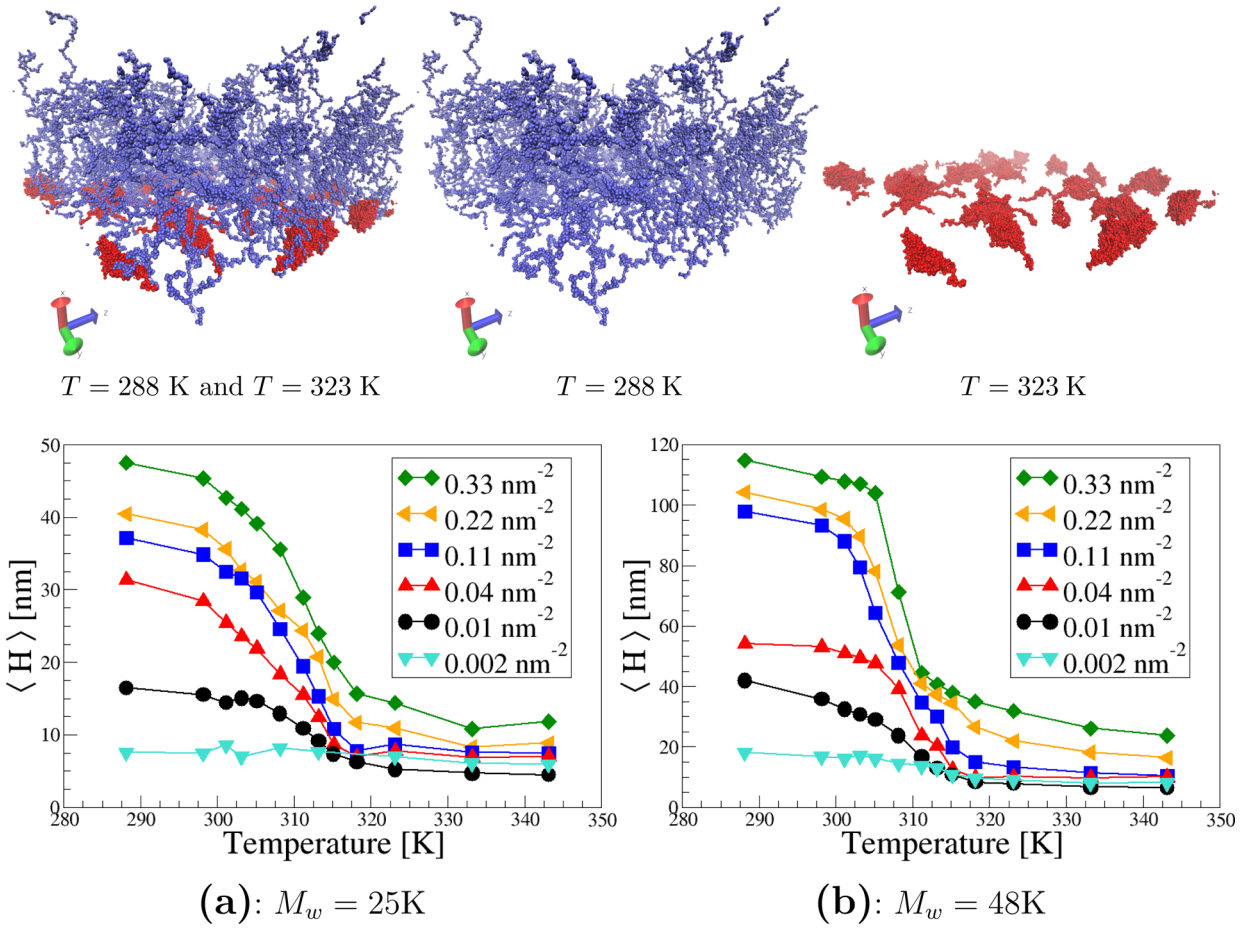

Figure 1. (Upper row) Snapshots of the chain conformations of PNIPAM polymers of weight M_w = 48 kDa and grafting density σ = 0.01 nm^{-2} below (T = 288 K) and above (T = 323 K) T^{LCST}. (Lower row) Swollen brush height for PNIPAM polymers of weights (a) M_w = 25K and (b) M_w = 48K as a function of the brush grafting density.

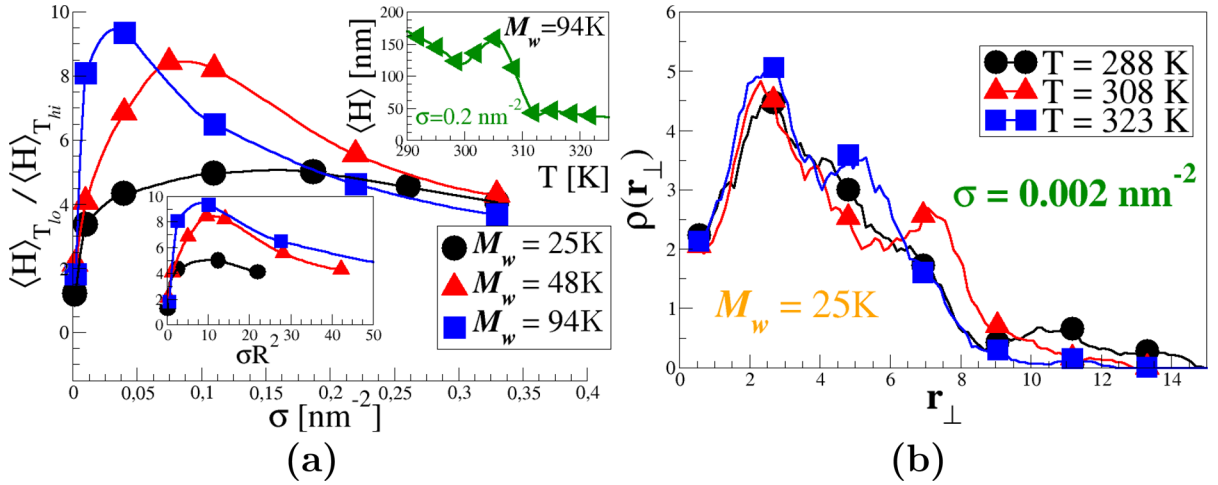

Figure 2. (a) Ratio of the brush thickness for temperatures T_{lo} = 293 K and T_{hi} = 333 K as a function of the grafting density (σ) and surface coverage σR_{ee}^2 at different polymer weights M_w. Inset: swollen brush thickness at σ = 0.2 nm^{-2} and M_w = 94K. (b) Number density profiles as a function of the distance $r_\perp$ to the grafting substrate for a brush of grafting density σ = 0.002 nm^{-2} and PNIPAMs of weight M_w = 25K. Temperatures below (288 K), around (308 K), and above (323 K) the T^{LCST} are depicted.

the parameters Θ = 307.81 K and W = 532.15 K, namely, $v_{AA}(T) = 31.41(1 - T/\Theta)$ and $w_{AAA}(T) = -2.93(1 - T/W)$. The resulting temperature-dependent Flory–Huggins compatibility parameter $\chi(T)$ is depicted in Figure 3.

In the upper row of Figure 1, we show the resulting chain conformations for a brush of grafting density σ = 0.01 nm^{-2} comprised of PNIPAM polymers of molecular weight M_w = 48K below and above the LCST at 288 and 323 K, respectively. In the latter regime (i.e., under poor solvent conditions), lateral chain

DOI: 10.1021/am5076309
ACS Appl. Mater. Interfaces 2015, 7, 12450–12462

aggregations that form "octopus micelles" are observed in agreement with experiments.[45−47] On the basis of unfavorable polymer−solvent surface tension, surface micelles or dimples are expected to appear when the grafted molecules begin to overlap.[4,48,49] In the snapshot on the right in Figure 1, we also observed collapsed globules formed by only a single chain. These fluctuations of the dimple sizes stem from the heterogeneities of the local surface coverage due to random grafting.

In the lower row of Figure 1, we plot the swelling behavior of pure PNIPAM brushes as a function of the grafting density for two different molecular weights. For M_w = 25K, the polymers are discretized into N^{CG} = 221 segments, whereas for M_w = 48K, the Gaussian chains contain N^{CG} = 424 units. For both systems, the segmental length is identical and is equal to $b^{CG} \simeq 0.55$ nm. In Figure 1, the average height of the brush $\langle H \rangle$ is obtained by estimating the first moment of the number density profiles $\rho(r_\perp) = L_\parallel^{-2} \int d\mathbf{r}_\parallel \rho(\mathbf{r}_\parallel, r_\perp)$; namely, $\langle H \rangle \equiv 2 \int r_\perp \rho(r_\perp)\, dr_\perp / \int \rho(r_\perp)\, dr_\perp$, where the factor 2 ensures that $\langle H \rangle$ reduces to the layer thickness for a step density profile.

In Figure 1a and b, we observe a decrease in the brush thickness both below and above the T^{LCST} with a transition region that becomes broader when the grafting density (σ) decreases.[7,50] Within that limit, polymer collapse is spread out, and the position of the critical temperature is difficult to define.[51] This effect is probably in part due to lowering of the interaction forces between polymer segments. When M_w decreases, the temperature variation of the brush height appears to be smoother than at higher molecular weights.[7] In the latter case, the sharpness of the transition is a consequence of stretching of the chains. Increased steric repulsion and a larger number of interacting elements result in a higher free-energy barrier between the swollen and collapsed states. The equilibrium brush profiles are the consequence of interplay between screening of the bottom layers from the aqueous solvent and slowing of the penetration of water inside the brush. As soon as water interacts with the inner, deeper brush layers, the brush deflates abruptly.

To rationalize these different trends, we plotted in Figure 2a the ratio of the brush thickness between the low and high temperature regimes for different polymer weights M_w as a function of the brush grafting density (σ). As also obtained from self-consistent-field (SCF) simulations[52] and observed experimentally,[6] this ratio depicts a maximum at an intermediate value of the grafting density (σ) whose magnitude increases with M_w and shifts to lower values as M_w increases. As already discussed, the strong dependence on M_w at an intermediate σ is due to stretching of the polymers. For high M_w, the grafting density at which the brush is maximally swollen is very low. In fact, for such systems, when we increase the grafting density, the swelling behavior and shape of the transition region are modified. This is shown in the inset of Figure 2a, where the swelling of a brush of grafting density σ = 0.2 nm^{-2} and polymers of M_w = 94K are presented and show an additional bump in the vicinity of the T^{LCST}. The experimental observation of this peak for high weight PNIPAM polymers with a large grafting density is often attributed to a vertical phase separation within the brush[53,54] with a dense layer close to the grafting substrate and a second layer that swells.[54] This picture comes from fitting of segment concentration profiles that are better achieved using bilayer functions. However, an unambiguous relationship between the peak and a bilayer profile is still a matter of debate,[6] and it is not clear if vertical phase separation is responsible for the presence of the peak. In our simulations, we also found no clear evidence of a bilayer profile.

Finally, at the very low surface density limit (i.e., σ = 0.002 nm^{-2}), we observed in Figure 1 that the change in polymer extension between the low and high temperature regimes for M_w = 25K is smaller than for M_w = 48K. This agrees with recent experimental observations in which this effect was attributed to conformations of PNIPAM chains that remain swollen, or collapse into single-chain globules, even above T^{LCST}.[6,51] The very low grafting density corresponding to the low polymer weight does not favor the collapse of neighboring chains into dimples or the emergence of a cooperative response to the solvent quality. The density profiles in Figure 2b seem to favor the existence of layering;[55] however, it should be noted that despite configurational averaging, the plots remain very noisy such that any conclusions about layering will remain unsettled.

4. MIXED PNIPAM:PEO BRUSH

Poly(ethylene oxide) (PEO) immersed in water exhibits a PNIPAM-like critical T^{LCST} that results from temperature-dependent changes in hydrogen bonding of the oxide groups. To account for this effect on the level of the virial coefficients, we make use of the solvation model proposed by Matsuyama et al.,[56] which has been revisited by Bekiranov et al.[57] In the simplest approach, the second- and third-order coefficients are written as

$$v_{BB}(\tau) = 1 - 2\chi(\tau) + \mathcal{L}(\tau)(2 + \mathcal{L}(\tau))$$
$$w_{BBB}(\tau) = 1 + \mathcal{L}^3(\tau)(4 + 3\mathcal{L}(\tau)) \quad (11)$$

where $\mathcal{L}(\tau) = \lambda(\tau)/(1 + \lambda(\tau))$, $\tau = 1 - \theta_0/T$, and $\chi(\tau) = 1/2 - \tau$. The characteristic temperature θ_0 is defined as $\chi(\theta_0) = 1/2$. A negative $v_{BB}(\tau)$ value corresponds to poor solvent conditions, and $v_{BB}(\tau) > 0$ corresponds to a good solvent. The energy barrier of hydrogen bonding is introduced through the relation $\lambda(\tau) = \lambda_0 e^{(\gamma(1-\tau))}$, where $\gamma = \Delta\varepsilon/(k_B\theta_0)$. In fact, this model can be used for a wide variety of hydrogen-bonding systems. For PEO, θ_0 = 730 K, γ = 6, and $\lambda_0 = 1.66 \times 10^{-5}$. The resulting Flory−Huggins parameter $\chi(T)$ for PEO is plotted in Figure 3.

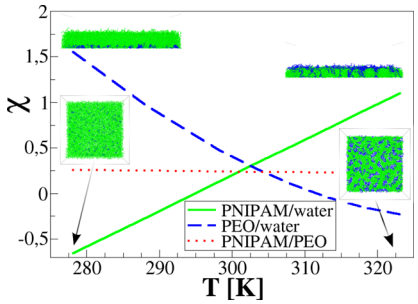

Figure 3. Temperature dependence of the the solvent-mediated $\chi_{\alpha S}(T)$ and interspecies $\chi_{\alpha\beta}(T)$ Flory−Huggins compatibility parameters as used in the simulations. Snapshots correspond to the side and top views of the equilibrated morphologies for a mixed brush of compositions f_A = 0.8 for PNIPAM and f_B = 0.2 for PEO with a grafting density of σ = 0.42 nm^{-2}.

In addition, the interspecies compatibility parameter has to be defined for mixed brushes. To this aim, we make use of the relation discussed in section 2.2 with the Hildebrand parameters δ_{PEO} = 20.2 (J/cm^3)$^{1/2}$ and δ_{PNIPAM} = 17.235 (J/cm^3)$^{1/2}$ at 303 K.[58] In fact, from the temperature dependence of the solvent-mediated interaction $\chi_{\alpha S}(T)$ depicted in Figure 3, we infer that

DOI: 10.1021/am5076309
ACS Appl. Mater. Interfaces 2015, 7, 12450−12462

the opposite trend of each species gives rise to a mixed interaction in our solvent-free model that depends on the temperature only weakly.

Here, we consider two systems that differ in the molecular weights of each species. System I consists of PNIPAM with $M_{w(A)}$ = 25K and PEO with $M_{w(B)}$ = 5K that are discretized into N_A^{CG} = 55 and N_B^{CG} = 38 interaction centers, respectively. The reference characteristic length scale is equal to 4.46 nm. System II aims to mimic the behavior of PNIPAM polymers with $M_{w(A)}$ = 94K and PEO with $M_{w(B)}$ = 18.8K. Each polymer is therefore represented by Gaussian chains of length N_A^{CG} = 208 and N_B^{CG} = 146 with a reference length of 6.12 nm.

Taking advantage of the particle-based representation of the M-DPD model, we consider polydisperse systems of fixed polydispersity index (PDI) $\equiv \langle (N_\alpha^{CG})^2 \rangle / \langle N_\alpha^{CG} \rangle^2 = 2$, where α = [A, B], in addition to the monodisperse case.

In the case of system I, three different grafting densities of the brush are considered at a fixed lateral extension $L_\parallel = 16R_{ee}$, denoted as $S(1)$: $\{\sigma = 0.21\ \text{nm}^{-2}\}$, $S(2)$: $\{\sigma = 0.42\ \text{nm}^{-2}\}$, and $S(3)$: $\{\sigma = 0.63\ \text{nm}^{-2}\}$, whereas for system II we deal only with a low grafting density $\sigma = 0.105\ \text{nm}^{-2}$. For each sample $S(i)$, the number of PNIPAM and PEO chains varies such that the overall grafting density of the brush remains constant. We therefore always fulfill the condition $f = \Sigma_\alpha f_\alpha \equiv 1$ by varying $f_B \in \{0; 0.2; 0.4; 0.6; 0.8\}$.

4.1. Effect of the Fraction of PEO. Figure 4 shows side and top views of mixed PNIPAM:PEO brushes for temperatures below (278 K) and above (323 K) T^{LCST} over three sets of grafting densities. To complement the snapshot, we provide more details about the density profiles $\rho(r_\perp)$ of each species as a function of the distance $r_\perp$ to the grafting substrate in Figure 5. We note that morphologies are obtained for relative fractions of PEO chains f_B = 0.2 and 0.8, the complement being filled by PNIPAM chains. At low temperature and independent of the grafting density (σ), PNIPAM chains dominate the brush structure because they are exposed to a good solvent. For systems with high PEO compositions, the dominance of PNIPAMs at the top of the brush is preserved but additional lateral segregation appears, which becomes stronger with low surface coverage. For such systems, as the temperature increases above the T^{LCST}, the vertical stratification switches and clear laterally segregated and collapsed domains are developed. By increasing σ, we observe more defined domains. With high PEO contents, PNIPAM chains collapse to form domains embedded in the PEO matrix. With small PEO content, PEO forms domains outside of a PNIPAM matrix.

A more qualitative characterization of the switching behavior and lateral structure formation of the domains can be achieved by computing the structure factor $S_c(\mathbf{q})$ for the composition contrasted between each species,[27,28] which is defined through

$$S_c(\mathbf{q}) = \left\langle \left| \sum_{i=1}^{n} \sum_{s=1}^{N_i} [\gamma_A(i, s) - \gamma_B(i, s)] e^{j\mathbf{q}(\mathbf{r}_i)} \right|^2 \right\rangle \quad (12)$$

where $\gamma_\alpha(i, s) = 1$ if the sth segment on the ith polymer chain belongs to species α; otherwise, $\gamma_\alpha(i, s) = 0$. Because of the translational invariance in the parallel directions (x, y), the structure factor $S_c(q_\perp, \mathbf{q}_\parallel)$ is circularly averaged over the parallel reciprocal vector $\mathbf{q}_\parallel$.

Figure 6a depicts the temperature dependence of the maximal intensity $(I_c(T))$ of $S_c(q)$ for the systems considered in Figures 4 and 5. This quantity should reveal the emergence of lateral

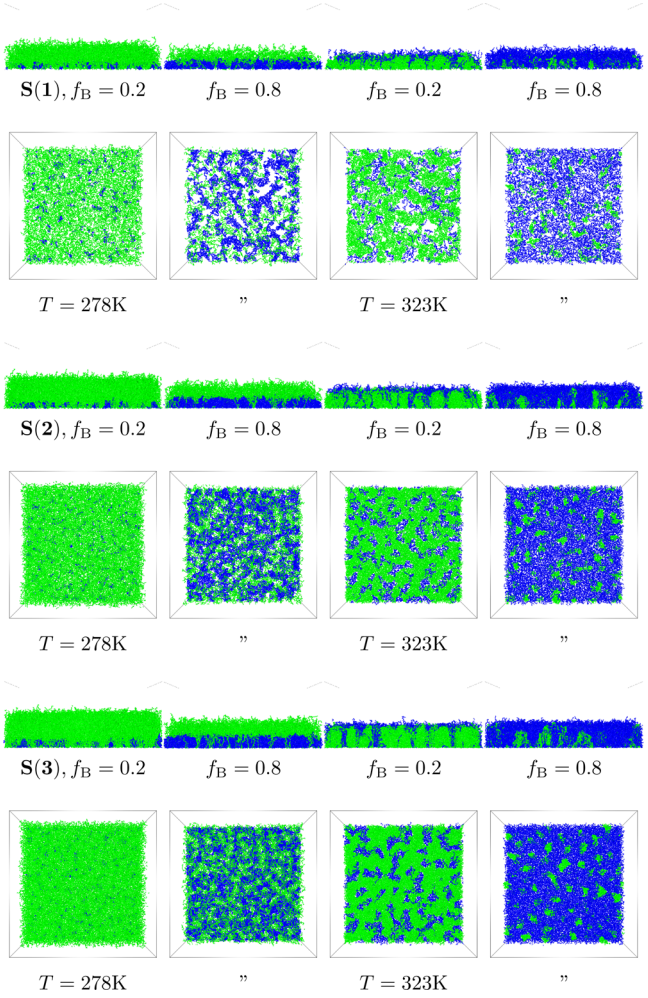

Figure 4. Side and top views of monodisperse mixed brushes of system I ($M_{w(A)}$ = 25K for PNIPAM and $M_{w(B)}$ = 5K for PEO). The temperature (T) of the water is varied below and above the T^{LCST}. The relative fraction of PEO chains is also varied between small (f_B = 0.2) and large (f_B = 0.8) amounts, and brushes of the grafting densities $S(1)$: $\{\sigma = 0.21\ \text{nm}^{-2}\}$, $S(2)$: $\{\sigma = 0.42\ \text{nm}^{-2}\}$, and $S(3)$: $\{\sigma = 0.63\ \text{nm}^{-2}\}$ are considered. PNIPAM chains are colored green, and PEO chains blue.

domains with different compositions. The structure factor of each species is plotted in Figure 6b to discriminate between the species that participate most in the formation of the domains. For $T < T^{LCST}$, the maximal intensity $I_c(T)$ has a higher magnitude for a large f_B fraction of PEO. The poor solvent conditions for PEO encourage the formation of PEO domains, and this effect is enhanced when the amount of PNIPAM is too small to shield the PEO chains from the aqueous solvent. From Figure 6b, we also see that increasing the grafting density favors the collapse of PEO chains at low f_B, whereas it alters their structure at high f_B. In this case, the domains percolate laterally over the sample. For $T \sim T^{LCST}$, PNIPAM components penetrate the brush, and PEO swells. PNIPAM chains create a top layer that is presumably a better solvent than water for PEO. During the temperature-induced transitions of each species, fluctuations in the compositions decrease, which leads to a smearing of $I_c(T)$. The intensity of the $I_c(T)$ decrease is higher at a high f_B fraction of PEO because many preformed PNIPAM domains are destroyed when the PEO polymers swell. Finally, for $T > T^{LCST}$, the composition contrast increases strongly because PNIPAM creates domains in the PEO matrix. This collapse is easier

DOI: 10.1021/am5076309
ACS Appl. Mater. Interfaces 2015, 7, 12450−12462

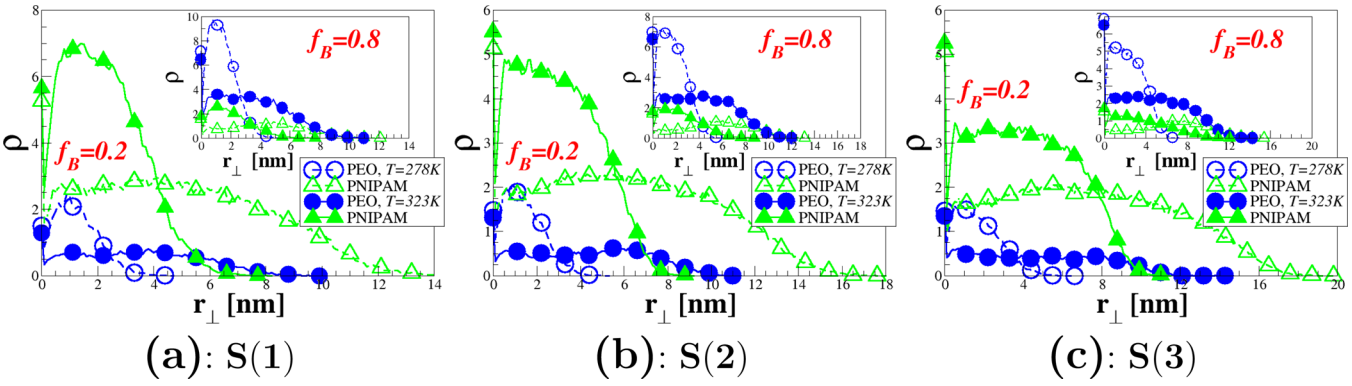

Figure 5. (a–c) Density profiles $\rho(r_\perp)$ of each species as a function of the distance $r_\perp$ to the bare substrate and for different compositions f_B. Open symbols are for $T < T^{LCST}$ and filled for $T > T^{LCST}$. These profiles were generated from the morphologies depicted in Figure 4.

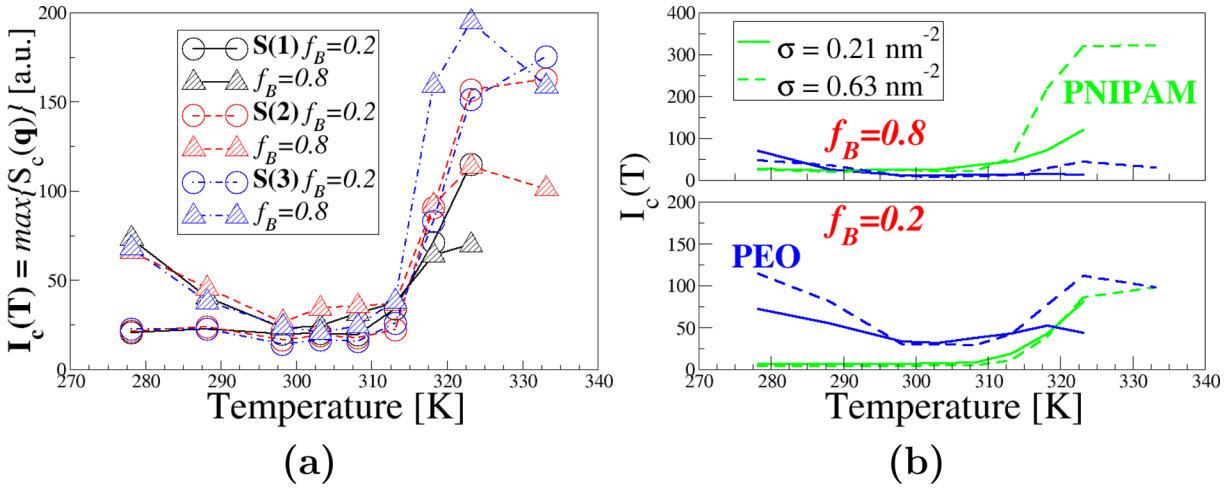

Figure 6. Maximal intensity of the structure factor $S_c(q)$ of the compositions using eq 12 for the systems depicted in Figures 4 and 5 computed for (a) both species and (b) each species independently.

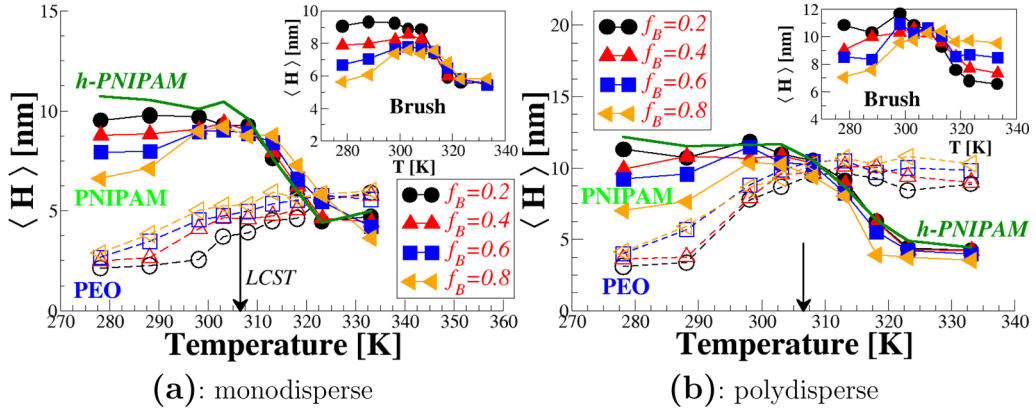

Figure 7. Swelling of mixed PNIPAM:PEO brushes of grafting density $\sigma = 0.63$ nm^{-2} as a function of the f_B fraction of PEO chains for (a) monodisperse and (b) polydisperse samples of PDI = 2. Measured average thickness of each species (primary panels) and average thickness of the whole brush (insets). The swelling behavior of the corresponding pure PNIPAM (*h-PNIPAM*) brush ($f_B = 0$) is also plotted. Filled symbols correspond to PNIPAM components, whereas empty symbols represent PEO components. Arrows mark the position of the T^{LCST}.

when the number of PNIPAM chains is smaller (i.e., high f_B), which explains the earlier increase of $I_c(T)$ for $f_B = 0.8$. As shown in Figure 6b, increased grafting density also boosts this effect. Conversely, for a large fraction of PNIPAM, well-defined PEO domains emerge on top of a rich PNIPAM matrix.

In Figure 7a and b, we plot the brush thickness of system $S(3)$ for (a) monodisperse and (b) polydisperse brushes. In the main panels of both figures, the average height $\langle H \rangle$ of each species and the corresponding swelling of the one-component PNIPAM brush ($f_B = 0$) are plotted; the insets depict the swelling of the total brush height. We first note that polydisperse systems depict a brush thickness at low temperature that is larger and a switching interval around T^{LCST} that is broader than those of the monodisperse brushes. Polydisperse brushes also depict higher,

DOI: 10.1021/am5076309
ACS Appl. Mater. Interfaces 2015, 7, 12450–12462

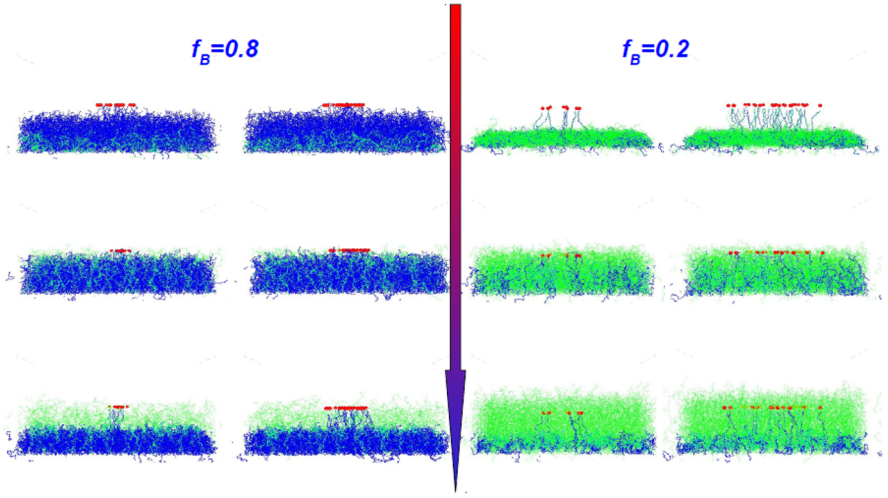

Snapshots at $T = 333$K (top), $T = 308$K (middle) and $T = 293$K (bottom row) for $\sigma = 0.105$ nm^{-2}.

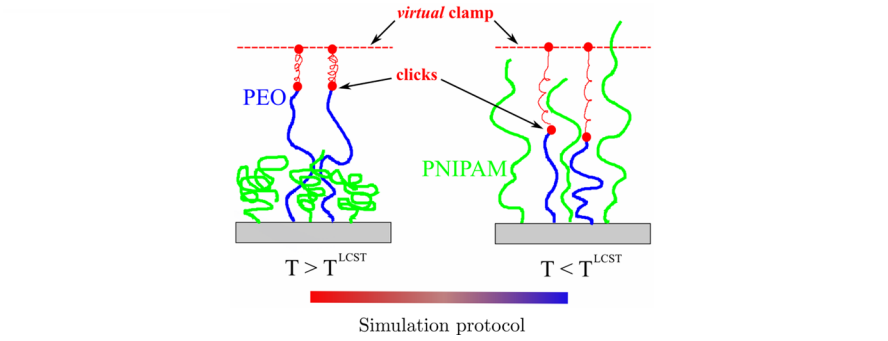

Figure 8. Sketch of the simulation setup. PEOs are clicked at $T > T^{LCST}$ to an immobile, virtual clamp (i.e., transparent to nonclicked polymers). The temperature is then decreased to reach the swollen state regime of PNIPAM. In simulations, the click parts of the clamp are permanently linked by a spring to the chain ends during cooling, and forces that act on the clamp are monitored. Snapshots depict side views of a cut section in the middle of a brush with PNIPAM weights of $M_{w(A)}$ = 94K and PEO $M_{w(B)}$ = 18.8K and a lateral extension of $L_{\|} \simeq 98$ nm.

sharper, earlier swelling of PEO species when the PNIPAMs inversely shrink. This observation can be attributed to facilitated penetration of the aqueous solvent because of the size polydispersity of both species. It also accentuates the swelling of PEO chains once they contact water. This effect is enhanced when the fraction of PEO chains $(f_B) > 0.5$, which is also visible (but weaker) in the case of the monodisperse system. Independent of the dispersity effects, we observe a decrease in the PNIPAM thickness when an increasing amount of PEO chains is added. For $T < T^{LCST}$, this is because of poor solvent conditions for PEO and likely concomitant shielding by PNIPAM. For $T > T^{LCST}$, the PEO brush height decreases as the fraction is increased because the density of chains is swollen by the good solvent, and the additional steric repulsion is reduced. For the polydisperse system, PEO chains are not shielded as well by PNIPAM, and size polydispersity facilitates penetration of water into the brush. This leads to an increase in the brush height when f_B increases in the polydisperse brush.

4.2. Response of PNIPAM:PEO Mixed Brushes to Local Forces Exerted by Adsorbed Biomolecules. Designing biofunctional materials necessitates understanding of protein and cell adhesion at interfaces. New materials with tailored surface topographies and chemistry are promising candidates and trigger more complex protein/substrate interactions allowing for repeatable, noninvasive, and nondestructive attachments to cells or proteins. One route to address these multiple constraints is to develop multicomponent polymer brushes with functional groups on one of the components of the brush.[59] For example, PNIPAM-*b*-PS:PEO mixed brushes or PNIPAM:PEO-*b*-PS in which a small hydrophobic polystyrene end-block (PS) strongly interacts with the hydrophobic domains of the biomacromolecule in solution could provide such functionality. The next challenge consists of being able to remove the nonanchored biomacromolecules from the surface on demand without removing the functional brush coating. This requires an understanding of the elastic properties of the brush surface (stresses, forces, and deformations) and the optimal amount and spatial distribution of anchors at the top of the brush, as well as how it depends on the surface coverage and possible lateral morphologies.

To address these questions, we considered PNIPAM:PEO mixed brushes with a fraction of the chain ends irreversibly connected to an immobile clamp. The numerical experiment is sketched in Figure 8, where PEO chains carry functional chain ends that we denote as clicks. In simulations, the chain ends are attached by a spring of stiffness $K_s = 1\ k_BT/\text{nm}^{-2}$ to an immobile clamp that is transparent to nonattached polymers. Each connection between the clamp and a chain end involves an immobile click (part of the clamp) and a mobile click connected to the polymer, which allows us to monitor the forces (F_s) exerted by the clicked chains on the clamp. Furthermore, we vary the number (n_c) of clicks, which are randomly distributed within a defined area, mimicking the effect of a single or multiple hydrophobic attachment(s) to the biomacromolecule. Finally,

DOI: 10.1021/am5076309
ACS Appl. Mater. Interfaces 2015, 7, 12450−12462

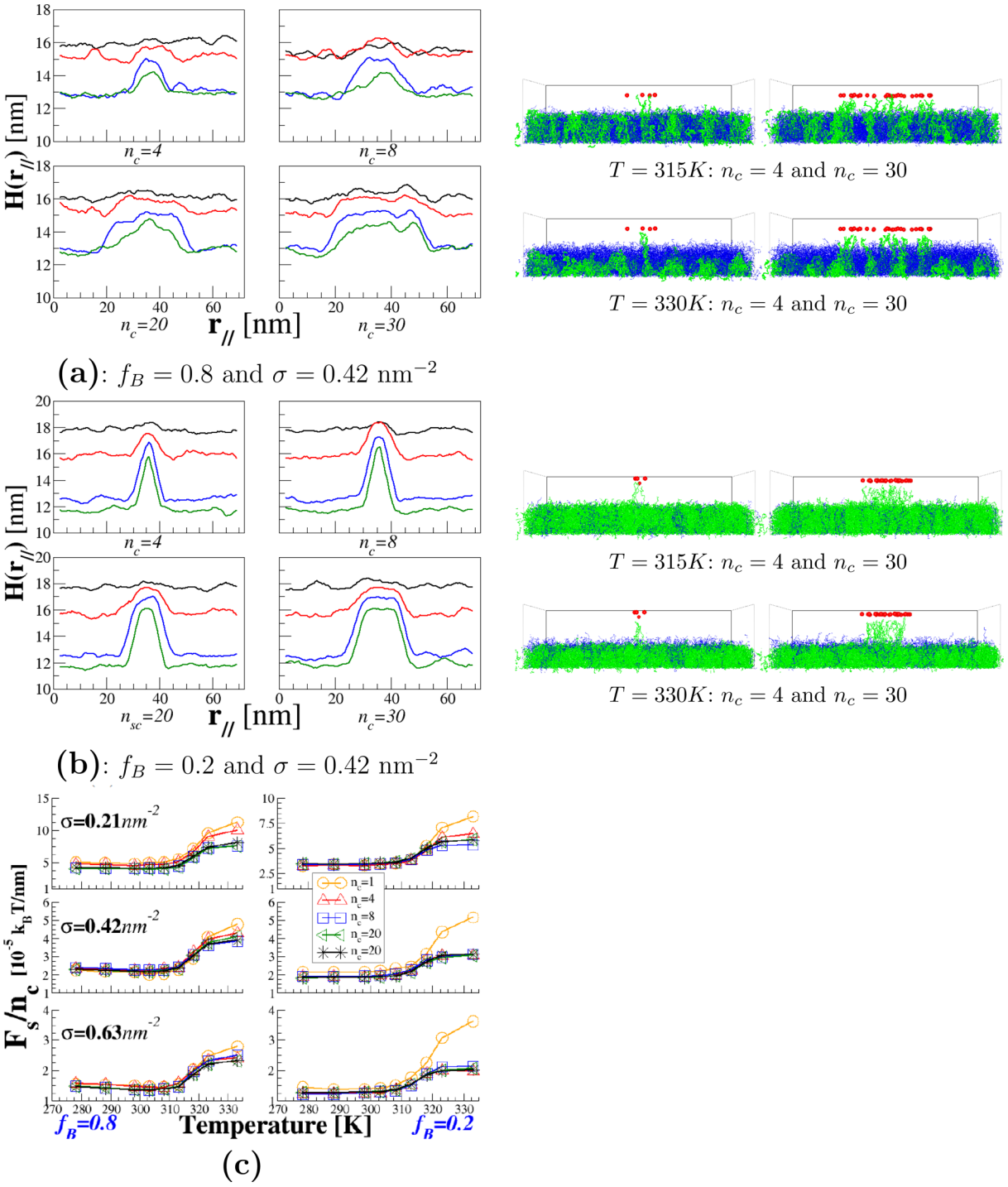

Figure 9. (a and b) Average brush surface profiles and corresponding snapshots when PNIPAM chains are clicked at differing n_c amounts of clicked PNIPAMs. Temperature decreases were monitored at 330, 315, 308, and 278 K. (c) The average force acting on the clamp as a function of temperature and number of clicks (n_c). The f_B ratio of PEO components is also varied. PNIPAM $M_{w(A)}$ = 25K, and PEO $M_{w(B)}$ = 5K.

the position $r_{\perp}^{clamp}$ of the clamp is chosen to be 1.5 nm above the maximal extent of the selected polymers within the defined area.

Here, we consider mixed brushes with an f_B fraction of PEO polymers and different brush grafting densities (σ). For each system, we chose to work at a fixed number of clicks (n_c) whose surface densities depended on the fraction of PEO in the brushes. At a fixed f_B fraction and different grafting densities (σ), we imposed the corresponding surface density of clicks $\sigma_c(f_B)$ to fulfill the constraint $\sigma_c(f_B)/\sigma \sim$ cste (constant). In addition, for two different fractions $f_B^{(1)}$ and $f_B^{(2)}$ at a fixed brush grafting density (σ), we chose the surface density of clicks to follow the relation $\sigma_c(f_B^{(1)}) = (f_B^{(2)}/f_B^{(1)})\sigma_c(f_B^{(2)})$.

4.2.1. Clicked PNIPAM Chains. We first consider the aforementioned system I (see Figure 4) (i.e., PNIPAM $M_{w(A)}$ = 25K and PEO $M_{w(B)}$ = 5K) for which the f_B fraction of PEO is fixed to either f_B = 0.2 or 0.8, and n_c PNIPAM polymers are connected to the clamp. For the system depicted in Figure 9, the brush grafting density is fixed at σ = 0.42 nm^{-2}, and we use $\sigma_c(f_B = 0.8) \simeq 0.04$. The clamp is located at $r_{\perp}^{clamp}(f_B = 0.8) \simeq 16.5$ nm and $r_{\perp}^{clamp}(f_B = 0.2) \simeq 18.5$ nm, and the lateral size of the brush is

DOI: 10.1021/am5076309
ACS Appl. Mater. Interfaces 2015, 7, 12450−12462

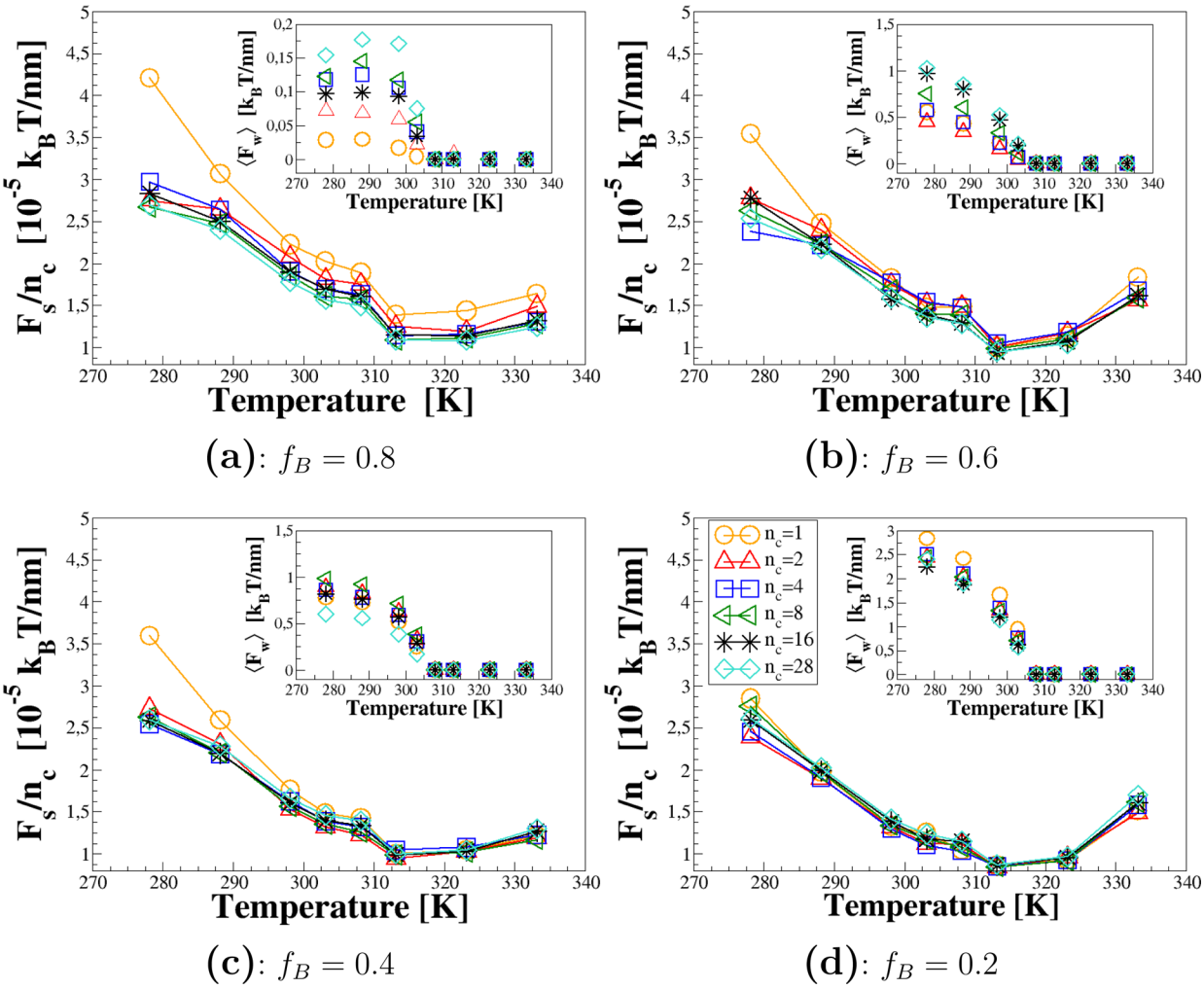

Figure 10. (a–d) Average force acting on the clamp when PEO chains are clicked as a function of temperature and number of clicks (n_c). The f_B ratio of PEO components is also varied. PNIPAM $M_{w(A)}$ = 94K, and PEO $M_{w(B)}$ = 18.8K. (insets) Average force that would be exerted by PNIPAM species on the clamp as a function of temperature.

$L_{\parallel} \simeq 71$ nm. Starting at 278 K ($<T^{LCST}$), the system is first equilibrated in the presence of clicks. The temperature is then increased by increments of 10 K; at each jump in temperature, the trajectories and forces that act on the clamp are collected during 2×10^5 molecular dynamics simulations (1000τ) until the temperature reaches 338 K ($\gg T^{LCST}$).

In Figure 9a and b, we plotted the average brush surface as a function of lateral coordinates for different temperatures along the cooling line and numbers of clicks. We observe a weaker deformation amplitude of PNIPAM domains upon heating when the fraction of PEOs is higher. When T increases, the solvent quality for PNIPAM changes from good to poor, giving rise to a chain collapse (see Figure 1); PEOs, on the other hand, experience the opposite trend. For high f_B and large n_c, the deformation of the brush surface below the clicks fixed on the clamp (see Figure 8 and the sketch of the simulation protocol) results from the overlap of a collection of individual PNIPAM chains, and the contours in Figure 9a depict widespread elevation. In Figure 9b, we also note narrowing of the deformed brush/solvent interface for small f_B and large n_c.

Figure 9c collects the average force on the clamp as a function of temperature, number of clicks (n_c), and brush grafting density (σ). When the temperature is reduced, the force–temperature curves strongly increase after the T^{LCST}, and it is immediately notable that pulling out one PNIPAM chain is always more costly than acting on many chains with increasing cost at low grafting density and higher strength when f_B is large. We also note that the magnitude of the force decreases when the grafting density increases. At high σ, it is easier for the clicked PNIPAM chains to optimize their interface energy with the solvent by building a larger interface and cooperatively deforming neighboring PNIPAM chains, which leads to a decrease in the resulting force acting on the clamp. These points show that neighboring chains that are collapsed near the pulled ones play an important role in decreasing the cost of deformation, and their contribution leads to additional elevation that surrounds the deformed and PNIPAM-rich domain.

4.2.2. Clicked PEO Chains. In Figure 8, we investigate the reverse system, namely, PEO chains clicked to the clamp at high temperature and for different f_B fractions of PEO. Following the same protocol as in section 4.2.1, the mixed brushes were then cooled by 10 K steps to reach the fully swollen state of PNIPAMs. Here, we consider polymers of system II as discussed in section 4, namely, PNIPAM of $M_{w(A)}$ = 94K, and PEO of $M_{w(B)}$ = 18.8K. Finally, because of the higher mass of the polymers, we consider a smaller grafting density $\sigma = 0.105$ nm^{-2} for the brush. The lateral size of the system is fixed to $L_{\parallel} \simeq 98$ nm, and we use a surface density of clicks $\sigma_c(f_B = 0.2) \simeq 0.045$. As before, the location of

DOI: 10.1021/am5076309
ACS Appl. Mater. Interfaces 2015, 7, 12450–12462

the clamp lies 1.5 nm above the maximal extent of the selected polymers, which means that, depending on f_B, its position varies between $r_\perp^{clamp}(f_B = 0.2) \simeq 25$ nm and $r_\perp^{clamp}(f_B = 0.8) \simeq 30$ nm.

In addition to the average force (F_s) exerted by the clicked PEO chains on the clamp, we also monitored the average force that PNIPAM polymers would exert if the clamp was a finite object and not transparent for the other species. For this purpose, we use a harmonic wall located at position $r_\perp^{wall} \equiv r_\perp^{clamp} + 30$ nm, where $r_\perp^{clamp}$ is the position of the clamp. The potential is written as $U_w = 0.5K_w(\Delta r_\perp - \Delta r_w^c)^2$ with $\Delta r_\perp = r_\perp^{wall} - r_\perp$ and $\Delta r_w^c = r_w^c + (r_\perp^{wall} - r_\perp^{clamp})$. The relative cutoff distance below the position of the clamp is fixed to $r_w^c = 1.224$ nm. Upon cooling, PNIPAM polymers swell and may reach the position $r_\perp^{clamp}$ of the clamp and eventually swell beyond it. Therefore, we obtained a very rough estimation of the force by computing the quantity $\langle F_w \rangle \equiv \int dr_\perp \rho_{(A)}(r_\perp) U_w'(r_\perp)$, where $\rho_{(A)}(r_\perp)$ represents the number density of PNIPAM polymers. Such a method allows for estimatation of the force that could be exerted by the other polymer species on the biomacromolecule to which the PEO chains are anchored.

The resulting force−temperature curves are depicted in Figure 10a−d. Starting from good solvent conditions for PEO, decreasing the temperature results in a transition to poor solvent conditions, whereas PNIPAM experiences the opposite trend. Keeping PEO chains under tension upon cooling results in an increase in the average force (F_s/n_c) acting on the clamp, and swelling of PNIPAM leads to an increase in the virtual force (F_w) that could act on the clamp. It also appears that F_s/n_c is rather independent of the amount of PEO at high temperature. Only at low temperatures does the force for $n_c = 1$ increase upon changing f_B from 0.2 to 0.8. It is again noteworthy that keeping one chain under tension is always more costly than acting on many chains, and that this cost decreases when the f_B number of PEO chains in the brush decreases. In contrast, the contribution of PNIPAMs to the force that acts on the clamp naturally increases. At high f_B, PEO forms laterally extended domains, and extracting one chain from such domains is more expensive than for a system with smaller, more dispersed domains, which is the case at small f_B. This reveals the importance of effective attractions in PEO-rich domains.

The insets in Figure 10 show how the force $\langle F_w \rangle$ that PNIPAM molecules exert on the clamp depends on n_c. The swelling of PNIPAM molecules upon cooling leads to an increasing contribution to $\langle F_w \rangle$. At low T, we observe an increase in the $\langle F_w \rangle$ magnitude with a decrease in f_B because the number density of PNIPAM also increases. At a large fraction of PNIPAM ($f_B = 0.2$), the magnitude for small n_c is larger than for high n_c, whereas this trend is inverted when the fraction of PNIPAM polymers decreases (increasing f_B). The reason is that at high f_B the deformed PEO domains are denser, and PNIPAMs have to avoid these domains to reach the aqueous solvent. As the size of the deformed domains increases, the barrier for PNIPAMs to cross is more costly. At small f_B, the domains are more dispersed, and increasing n_c results more in deforming many small PEO domains. The cost may therefore behave as the sum of contributions of crossing singular-like domains of PEO.

As noted for clicked PNIPAMs, the force that acts on one clamp always results from the contribution of neighboring chains of the same species (i.e., the cost of deforming the whole domain). It turns out that the additional elevation surrounding pulling out a single PEO chain involves a cost that is dependent on the composition of the species. High f_B leads to contributions that are higher than at small f_B.

5. SUMMARY

In this work, we used molecular dynamics simulations of a soft, coarse-grained model with an implicitly treated solvent to explore the temperature response of PNIPAM-based pure and mixed brushes. The model can represent experimentally large, invariant degrees of polymerization that can account for realistic fluctuations. In contrast to previous work that employed a collocation grid to compute density-dependent nonbonded interactions,[60,61] we used multiple dissipative particle dynamics (M-DPD)[33−35] that does not break translational invariance. This allowed us to evaluate the force and displacement response of the polymers to a prototypical biomacromolecule.

In a first part of this study, we investigated the ability of the model to reproduce the temperature-induced swelling of pure PNIPAM polymers of different molecular weights as a function of the brush grafting density. In agreement with previous experiments[7,50] and numerical works,[52] we observe sharpening of the collapse upon heating as we increase the molecular weight of the grafted chains or increase the grafting density. Sharpening of the transition between the low and high temperature states when the grafting density increases, and the dependence of the transition on the molecular weight of the polymer, confirmed the model as it relates to experimental observations. Limited to low grafting densities, we find evidence for the formation of complex, lateral, and localized structures (dimples). For high molecular weight and grafting density, we observe maximum swelling of the brush in the transition regime without evidence for the presence of a vertical phase separation.

In the second part of this study, we examined the conformational properties of PNIPAM-based mixed brushes after incorporating various amounts of a temperature-sensitive polymer (PEO) that exhibits a swelling behavior that is antagonistic to that of PNIPAM. Brushes of different grafting densities and relatively low molecular weights were studied, and mono- and polydisperse brushes were considered. We find the development of complementary morphologies for both species depending on the temperature relative to the T^{LCST} and the number of PEO chains in the brush. In particular, increasing the fraction of PEO chains strongly modifies swelling of the brush in the temperature range below and around the T^{LCST}. In addition to this effect, polydispersity increases the height of the brush above the T^{LCST} with a magnitude that increases with the fraction of PEO.

In the last part of this study, the response of the mixed brushes to a local constraint acting on one of the species was investigated. The choice of the constraint was intended to mimic the presence of a biomacromolecule that preferentially interacts with the functionalized ends of the brush molecules. First, various numbers of PNIPAM chain ends were pulled out of the brush as the temperature increased toward the T^{LCST}. We found that the cost of deforming a single PNIPAM molecule was always higher than for larger domains with a strength that increased with the fraction of PEO. Furthermore, the cost of deformation at low grafting density was always found to be higher than at high grafting density. Second, PEO chains were used to support the constraint while the temperature was decreased from above to below the T^{LCST}. We find that neighboring PEO molecules collapse around the polymers that carry the constraints, leading to surrounding molecules being elevated. The cost of deformation was also found to increase with the fraction of PEO.

Our findings provide a basis for further simulations by elucidating general mechanisms that control the morphology of

DOI: 10.1021/am5076309
ACS Appl. Mater. Interfaces 2015, 7, 12450−12462

thermoresponsive multicomponent polymer brushes. The simulation model and strategy are well suited to capture relevant parameters, and more importantly, the same form of density functional of nonbonded interactions has been shown to devise a solvent-free model for lipid membranes,[31,62,63] allowing us to study mixed polymer brushes in contact with a lipid membrane within a unified framework. The last part of this study is intended to elucidate fundamentals for such systems. Finally, the versatility of the model allows for consideration of more complex and realistic mixing of the polymer species. In particular, given the Flory–Huggins effective interactions,[64] mixed pH and thermoresponsive brushes could be envisaged[65] with or without functional chain ends.[59]

AUTHOR INFORMATION

Corresponding Authors

*E-mail: leonforte@theorie.physik.uni-goettingen.de.

*E-mail: mmueller@theorie.physik.uni-goettingen.de.

Notes

The authors declare no competing financial interest.

ACKNOWLEDGMENTS

It is with great pleasure we thank S. Minko, I. Luzinov, A. Revzin, K. Hinrichs, P. Uhlmann, K. J. Eichhorn, and M. Stamm for stimulating discussions. Ample computer time at the Supercomputer Center (JSC), Jülich, HLRN Hannover and Berlin, as well as the GWDG Götingen are gratefully acknowledged. Financial support has been provided by the German Science Foundation within the DFG-NSF Materials World Network (Mu1674/12) and the Lichtenberg Program of the Volkswagen Foundation.

REFERENCES

(1) Heskins, M.; Guillet, J. Solution Properties of Poly(*N*-isopropylacrylamide). *J. Macromol. Sci., Part A: Pure Appl. Chem.* **1968**, *2*, 1441–1455.

(2) Taylor, L.; Cerankowski, L. Preparation of Films Exhibiting a Balanced Temperature Dependence to Permeation by Aqueous Solutions — a Study of Lower Consolute Behavior. *J. Polym. Sci., Polym. Chem. Ed.* **1975**, *13*, 2551–2570.

(3) Cheng, H.; Shen, L.; Wu, C. LLS and FTIR Studies on the Hysteresis in Association and Dissociation of Poly(*N*-isopropylacrylamide) Chains in Water. *Macromolecules* **2006**, *39*, 2325–2329.

(4) Choi, B.-C.; Choi, S.; Leckband, D. Poly(*N*-isopropyl acrylamide) Brush Topography: Dependence on Grafting Conditions and Temperature. *Langmuir* **2013**, *29*, 5841–5850.

(5) Plunkett, K.; Zhu, X.; Moore, J.; Leckband, D. PNIPAM Chain Collapse Depends on the Molecular Weight and Grafting Density. *Langmuir* **2006**, *22*, 4259–4266.

(6) Yim, H.; Kent, M.; Mendez, S.; Lopez, G.; Satija, S.; Seo, Y. Effects of Grafting Density and Molecular Weight on the Temperature-Dependent Conformational Change of Poly(*N*-isopropylacrylamide) Grafted Chains in Water. *Macromolecules* **2006**, *39*, 3420–3426.

(7) Bittrich, E.; Burkert, S.; Müller, M.; Eichhorn, K.-J.; Stamm, M.; Uhlmann, P. Temperature-Sensitive Swelling of Poly(*N*-isopropylacrylamide) Brushes with Low Molecular Weight and Grafting Density. *Langmuir* **2012**, *28*, 3439–3448.

(8) Cohen Stuart, M.; Huck, W.; Genzer, J.; Müller, M.; Ober, C.; Stamm, M.; Sukhorukov, G.; Szleifer, I.; Tsukruk, V.; Urban, M.; Winnik, F.; Zauscher, A.; Luzinov, I.; Minko, S. Emerging Applications of Stimuli-Responsive Polymer Materials. *Nat. Mater.* **2010**, *9*, 101–113.

(9) Nitschke, M.; Gramm, S.; Götze, T.; Valtink, M.; Drichel, J.; Voit, B.; Engelmann, K.; Werner, C. Thermo-Responsive Poly(NiPAAm-co-DEGMA) Substrates for Gentle Harvest of Human Corneal Endothelial Cell Sheets. *J. Biomed. Mater. Res., Part A* **2007**, *80*, 1003–1010.

(10) Halperin, A. Polymer Brushes that Resist Adsorption of Model Proteins: Design Parameters. *Langmuir* **1999**, *15*, 2525–2533.

(11) Hoffman, A. Applications of Thermally Reversible Polymers and Hydrogels in Therapeutics and Diagnostics. *J. Controlled Release* **1987**, *6*, 297–305.

(12) Lim, Y.; Kim, D.; Lee, D. Drug Releasing Characteristics of Thermo- and pH-Sensitive Interpenetrating Polymer Networks Based on Poly(*N*-isopropylacrylamide). *J. Appl. Polym. Sci.* **1997**, *64*, 2647–2655.

(13) Clara-Rahola, J.; Fernandez-Nieves, A.; Sierra-Martin, B.; South, A.; Lyon, L.; Kohlbrecher, J.; Fernandez Barbero, A. Structural Properties of Thermoresponsive Poly(*N*-isopropylacrylamide)–Poly(ethyleneglycol) Microgels. *J. Chem. Phys.* **2012**, *136*, 214903–214910.

(14) Gan, D.; Lyon, L. Synthesis and Protein Adsorption Resistance of PEG-Modified Poly(*N*-isopropylacrylamide) Core/Shell Microgels. *Macromolecules* **2002**, *35*, 9634–9639.

(15) Huang, Y.-Y.; Chung, T.-W.; Tzeng, T.-w. Drug Release from PLA:PEG Microparticulates. *Int. J. Pharm. (Amsterdam, Neth.)* **1997**, *156*, 9–15.

(16) Currie, E.; der Gucht, J.; Borisov, O.; Cohen-Stuart, M. Stuffed Brushes: Theory and Experiment. *Pure Appl. Chem.* **1999**, *71*, 1227–1241.

(17) Seeber, M. Synthesis and Characterization of Thermally Responsive Polymer Layers. Ph.D. Thesis, Clemson University, Clemson, SC, 2013.

(18) Virtanen, J.; Baron, C.; Tenhu, H. Grafting of Poly(*N*-isopropylacrylamide) with Poly(ethylene oxide) under Various Reaction Conditions. *Macromolecules* **2000**, *33*, 336–341.

(19) Virtanen, J.; Tenhu, H. Thermal Properties of Poly(*N*-isopropylacrylamide)–g–Poly(ethylene oxide) in Aqueous Solutions: Influence of the Number and Distribution of the Grafts. *Macromolecules* **2000**, *33*, 5970–5975.

(20) Matsen, M. The Standard Gaussian Model for Block Copolymer Melts. *J. Phys.: Condens. Matter* **2002**, *14*, R21–R47.

(21) Müller-Plathe, F. Coarse-Graining in Polymer Simulation: From the Atomistic to the Mesoscopic Scale and Back. *ChemPhysChem* **2002**, *3*, 754–769.

(22) Praprotnik, M.; Delle Site, L.; Kremer, K. Multiscale Simulation of Soft Matter: from Scale Bridging to Adaptive Resolution. *Annu. Rev. Phys. Chem.* **2008**, *59*, 545–571.

(23) Grest, G.; Murat, M. Structure of Grafted Polymeric Brushes in Solvents of Varying Quality: a Molecular Dynamics Study. *Macromolecules* **1993**, *26*, 3108–3117.

(24) Merlitz, H.; He, G.-L.; Sommer, J.-U.; Wu, C.-X. Reversibly Switchable Polymer Brushes with Hydrophobic/Hydrophilic Behavior: a Langevin Dynamics Study. *Macromolecules* **2009**, *42*, 445–451.

(25) Binder, K.; Kreer, T.; Milchev, A. Polymer Brushes under Flow and in other Out-Of-Equilibrium Conditions. *Soft Matter* **2011**, *7*, 7159–7172.

(26) Carillo, J.-M. Y.; Brown, W. M.; Dobrynin, A. V. Explicit Solvent Simulations of Friction between Brush Layers of Charged and Neutral Bottle-Brush Macromolecules. *Macromolecules* **2012**, *45*, 8880–8891.

(27) Wang, J.; Müller, M. Microphase Separation of Mixed Polymer Brushes: Dependence of the Morphology on Grafting Density, Composition, Chain-Length Asymmetry, Solvent Quality, and Selectivity. *J. Phys. Chem. B* **2009**, *113*, 11384–11402.

(28) Wang, J.; Müller, M. Microphase Separation of Diblock Copolymer Brushes in Selective Solvents: Single-Chain-in-Mean-Field Simulations and Integral Geometry Analysis. *Macromolecules* **2009**, *42*, 2251–2264.

(29) Plimpton, S. Fast Parallel Algorithms for Short-Range Molecular Dynamics. *J. Comput. Phys.* **1995**, *117*, 1–19.

(30) Lefevre, N.; Daoulas, K.; Müller, M.; Gohy, J.-F.; Fustin, C. Self-Assembly in Thin Films of Mixtures of Block Copolymers and Homopolymers Interacting by Hydrogen Bonds. *Macromolecules* **2010**, *43*, 7734–7743.

(31) Hömberg, M.; Müller, M. Main Phase Transition in Lipid Bilayers: Phase Coexistence and Line Tension in a Soft, Solvent-Free, Coarse-Grained Model. *J. Chem. Phys.* **2010**, *132*, 155104.

DOI: 10.1021/am5076309
ACS Appl. Mater. Interfaces 2015, 7, 12450–12462

(32) Müller, M.; MacDowell, L.; Yethiraj, A. Short Chains at Surfaces and Interfaces: a Quantitative Comparison Between Density-Functional Theories and Monte Carlo Simulations. *J. Chem. Phys.* **2003**, *118*, 2929.
(33) Pagonabarraga, I.; Frenkel, D. Dissipative Particle Dynamics for Interacting Systems. *J. Chem. Phys.* **2001**, *115*, 5015−5026.
(34) Trofimov, S.; Nies, E.; Michels, M. Thermodynamic Consistency in Dissipative Particle Dynamics Simulations of Strongly Nonideal Liquids and Liquid Mixtures. *J. Chem. Phys.* **2002**, *117*, 9383−9394.
(35) Trofimov, S.; Nies, E.; Michels, M. Constant-Pressure Simulations with Dissipative Particle Dynamics. *J. Chem. Phys.* **2005**, *123*, 144102.
(36) Hoogerbrugge, P.; Koelman, J. Simulating Microscopic Hydrodynamic Phenomena with Dissipative Particle Dynamics. *Europhys. Lett.* **1992**, *19*, 155.
(37) Espanol, P.; Warren, P. Statistical Mechanics of Dissipative Particle Dynamics. *Europhys. Lett.* **1995**, *30*, 191.
(38) Hildebrandt, J.; Scott, R. *The Solubility of Non-Electrolytes*, 3rd ed.; Reinhold: New York, 1950.
(39) Madkour, T. A Combined Statistical Mechanics and Molecular Dynamics Approach for the Evaluation of the Miscibility of Polymers in Good, Poor and Non-Solvents. *Chem. Phys.* **2001**, *274*, 187.
(40) Afroze, F.; Nies, E.; Berghmans, H. Phase Transitions in the System Poly(*N*-isopropylacrylamide)/water and Swelling Behaviour of the Corresponding Networks. *J. Mol. Struct.* **2000**, *554*, 55−68.
(41) Baulin, V.; Halperin, A. Signatures of a Concentration-Dependent Flory χ Parameter: Swelling and Collapse of Coils and Brushes. *Macromol. Theory Simul.* **2003**, *12*, 549−559.
(42) Baulin, V.; Zhulina, E.; Halperin, A. Self-Consistent Field Theory of Brushes of Neutral Water-Soluble Polymers. *J. Chem. Phys.* **2003**, *119*, 10977.
(43) Halperin, A.; Kröger, M. Collapse of Thermoresponsive Brushes and the Tuning of Protein Adsorption. *Macromolecules* **2011**, *44*, 6986−7005.
(44) Halperin, A.; Kröger, M. Thermoresponsive Cell Culture Substrates Based on PNIPAM Brushes Functionalized with Adhesion Peptides: Theoretical Considerations of Mechanism and Design. *Langmuir* **2012**, *28*, 16623−16637.
(45) Zhao, W.; Krausch, G.; Rafailovich, M.; Sokolov, J. Lateral Structure of a Grafted Polymer Layer in a Poor Solvent. *Macromolecules* **1994**, *27*, 2933−2935.
(46) Ishida, N.; Biggs, S. Effect of Grafting Density on Phase Transition Behavior for Poly(*N*-isopropylacryamide) Brushes in Aqueous Solutions Studied by AFM and QCM-D. *Macromolecules* **2010**, *43*, 7269−7276.
(47) Ishida, N.; Biggs, S. Direct Observation of the Phase Transition for a Poly(*N*-isopropylacryamide) Layer Grafted onto a Solid Surface by AFM and QCM-D. *Langmuir* **2007**, *23*, 11083−11088.
(48) Zhulina, E.; Birshtein, T.; Piramitsyn, V.; Klushin, L. Inhomogeneous Structure of Collapsed Polymer Brushes Under Deformation. *Macromolecules* **1995**, *28*, 8612−8620.
(49) Williams, D. Grafted Polymers in Bad Solvents: Octopus Surface Micelles. *J. Phys. II* **1993**, *3*, 1313.
(50) Takei, Y.; Aoki, T.; Sanui, K.; Ogata, N.; Sakurai, Y.; Okano, T. Dynamic Contact Angle Measurement of Temperature-Responsive Surface Properties for Poly(*N*-isopropylacrylamide) Grafted Surfaces. *Macromolecules* **1994**, *27*, 6163−6166.
(51) Zhu, X.; Yan, C.; Winnick, F.; Leckband, L. End-Grafted Low-Molecular-Weight PNIPAM Does Not Collapse above the LCST. *Langmuir* **2007**, *23*, 162−169.
(52) Mendez, S.; Curro, J.; McCoy, J.; Lopez, G. Computational Modeling of the Temperature-Induced Structural Changes of Tethered Poly(*N*-isopropylacrylamide) with Self-Consistent Field Theory. *Macromolecules* **2005**, *38*, 174−181.
(53) Yim, H.; Kent, M.; Mendez, S.; Balamurugan, S.; Balamurugan, S.; Lopez, G.; Satija, S. Temperature-Dependent Conformational Change of PNIPAM Grafted Chains at High Surface Density in Water. *Macromolecules* **2004**, *37*, 1994−1997.
(54) Yim, H.; Kent, M.; Satija, S.; Mendez, S.; Balamurugan, S.; Balamurugan, S.; Lopez, G. Evidence for Vertical Phase Separation in Densely Grafted, High-Molecular-Weight Poly(*N*-isopropylacrylamide) Brushes in Water. *Phys. Rev. E* **2005**, *72*, 051801.
(55) Yim, H.; Kent, M.; Huber, D. Conformation of End-Tethered PNIPAM Chains in Water and in Acetone by Neutron Reflectivity. *Macromolecules* **2003**, *36*, 5244−5251.
(56) Matsuyama, A.; Tanaka, F. Theory of Solvation-Induced Reentrant Phase Separation in Polymer Solutions. *Phys. Rev. Lett.* **1990**, *65*, 341.
(57) Bekiranov, S.; Bruinsma, R.; Pincus, P. Solution Behavior of Polyethylene Oxide in Water as a Function of Temperature and Pressure. *Phys. Rev. E* **1997**, *55*, 577−585.
(58) Mark, J. *Physical Properties of Polymers Handbook*, 3rd ed.; Springer: New York, 2007; Chapter 16, pp 289−303.
(59) Romeis, D.; Sommer, J.-U. Conformational Switching of Modified Guest Chains in Polymer Brushes. *J. Chem. Phys.* **2013**, *139*, 044910.
(60) Müller, M.; Smith, G. Phase Separation in Binary Mixtures Containing Polymers: A Quantitative Comparison of Single-Chain-in-Mean-Field Simulations and Computer Simulations of the Corresponding Multichain Systems. *J. Polym. Sci., Part B: Polym. Phys.* **2005**, *43*, 934−958.
(61) Daoulas, K.; Müller, M.; De Pablo, J.; Nealey, P.; Smith, G. Morphology of Multi-Component Polymer Systems: Single Chain in Mean Field Simulation Studies. *Soft Matter* **2006**, *2*, 573−583.
(62) Daoulas, K.; Müller, M. Polymer-Tethered Biomolecular Lipid Membranes. *Adv. Polym. Sci.* **2010**, *224*, 197−233.
(63) Fuhrmans, M.; Müller, M. Mechanisms of Vesicle Spreading on Surfaces: Coarse-Grained Simulations. *Langmuir* **2013**, *29*, 4335−4349.
(64) Sing, C.; De la Cruz, M. Polyelectrolyte Blends and Nontrivial Behavior in Effective Flory−Huggins Parameters. *ACS Macro Lett.* **2014**, *3*, 698−702.
(65) Tagliazucchi, M.; Li, X.; De la Cruz, M.; Szleifer, I. Self-Organized Polyelectrolyte End-Grafted Layers Under Nanoconfinement. *ACS Nano* **2014**, *8*, 9998−10008.

DOI: 10.1021/am5076309
ACS Appl. Mater. Interfaces 2015, 7, 12450−12462